Crystal Chemistry and Physical Properties of Superconducting and Semiconducting Charge Transfer Salts of the Type (BEDT-TTF)$_4$[$A^IM^{III}(C_2O_4)_3$]·PhCN (A^I = H_3O, NH_4, K; M^{III} = Cr, Fe, Co, Al; BEDT-TTF = Bis(ethylenedithio)tetrathiafulvalene)

Lee Martin,[†] Scott S. Turner,*[,†] Peter Day,*[,†] Philippe Guionneau,[‡] Judith A. K. Howard,[§] Dai E. Hibbs,[||] Mark E. Light,[||] Michael B. Hursthouse,[||] Mikio Uruichi,[⊥] and Kyuyo Yakushi[⊥]

Davy-Faraday Research Laboratory, The Royal Institution of Great Britain, 21 Albemarle Street, London, W1X 4BS, U.K., Laboratoire des Sciences Moleculaires, Institut de Chimie de la Matière Condensée de Bordeaux, 33608 Pessac Cedex, France, Department of Chemistry, University of Durham, South Road, Durham, DH1 3LE, U.K., Chemistry Department, University of Southampton, Highfield, Southampton, SO17 1BJ, U.K., and Institute of Molecular Sciences, Myodaichi, Okazaki, 444 Japan

Received October 31, 2000

Synthesis, structure determination by single-crystal X-ray diffraction, and physical properties are reported and compared for superconducting and semiconducting molecular charge-transfer salts with stoichiometry (BEDT-TTF)$_4$[$A^IM^{III}(C_2O_4)_3$]·PhCN, where A^I = H_3O, NH_4, K; M^{III} = Cr, Fe, Co, Al; BEDT-TTF = bis(ethylenedithio) tetrathiafulvalene. Attempts to substitute M^{III} with Ti, Ru, Rh, or Gd are also described. New compounds with M = Co and Al are prepared and detailed structural comparisons are made across the whole series. Compounds with A = H_3O^+ and M = Cr, Fe are monoclinic (space group *C*2/*c*), at 150, 120 K a = 10.240(1) Å, 10.232(12) Å; b = 19.965(1) Å, 20.04(3) Å; c = 34.905(1) Å, 34.97(2) Å; β = 93.69(1)°, 93.25(11)°, respectively, both with Z = 4. These salts are metallic at room temperature, becoming superconducting at 5.5(5) or 8.5(5) K, respectively. A polymorph with A = H_3O^+ and M = Cr is orthorhombic (*Pbcn*) with a = 10.371(2) Å, b = 19.518(3) Å, c = 35.646(3) Å, and Z = 4 at 150 K. When A = NH_4^+, M = Fe, Co, Al, the compounds are also orthorhombic (*Pbcn*), with a = 10.370(5) Å, 10.340(1) Å, 10.318(7) Å; b = 19.588(12) Å, 19.502(1) Å, 19.460(4) Å; c = 35.790(8) Å, 35.768(1) Å, 35.808(8) Å at 150 K, respectively, with Z = 4. All of the *Pbcn* phases are semiconducting with activation energies between 0.15 and 0.22 eV. For those compounds which are thought to contain H_3O^+, Raman spectroscopy or C=C and C−S bond lengths of the BEDT-TTF molecules confirm the presence of H_3O^+ rather than H_2O. In the monoclinic compounds the BEDT-TTF molecules adopt a β'' packing motif while in the orthorhombic phases $(BEDT\text{-}TTF)_2$ dimers are surrounded by monomers. Raman spectra and bond length analysis for the latter confirm that each molecule of the dimer has a charge of +1 while the remaining donors are neutral. All of the compounds contain approximately hexagonal honeycomb layers of $[AM(C_2O_4)_3]$ and PhCN, with the solvent occupying a cavity bounded by $[M(C_2O_4)_3]^{3-}$ and A. In the monoclinic series each layer contains one enantiomeric conformation of the chiral $[M(C_2O_4)_3]^{3-}$ anions with alternate layers having opposite chirality, whereas in the orthorhombic series the enantiomers form chains within each layer. Analysis of the supramolecular organization at the interface between the cation and anion layers shows that this difference is responsible for the two different BEDT-TTF packing motifs, as a consequence of weak H-bonding interactions between the terminal ethylene groups in the donor and the $[M(C_2O_4)_3]^{3-}$ oxygen atoms.

Introduction

Since the 1957 report by Ginzburg,[1] which set out the conditions under which superconductivity could occur in magnetic materials, there have been numerous efforts by solid-state chemists to synthesize superconducting compounds containing arrays of magnetic ions. Among the earliest were the ternary borides such as $ErRh_4B_4$,[2] followed by the Chevrel phases, e.g., $Pb_xSn_{1-x}Mo_6S_8$[3] and the borocarbides $ErNi_2B_2C$.[4] Most recent is $RuSr_2GdCu_2O_8$,[5] which becomes ferromagnetically ordered at a temperature (132 K) well above its superconducting T_c (40 K).[6] Apart from the last example, all these systems involve exclusively 4f moments, so it is pertinent to search for highly conducting compounds containing magnetic 3d ions. A potentially fertile area is that of molecular-based charge-transfer salts, where the first superconducting example was reported as long ago as 1981.[7] In such salts organochalcogenide donor molecules form the cations and may be combined with a wide variety of inorganic or organic anions.

* E-mail: sst@ri.ac.uk, pday@ri.ac.uk.
[†] Davy-Faraday Research Laboratory.
[‡] Institut de Chimie de la Matière Condensée de Bordeaux.
[§] University of Durham.
[||] University of Southampton.
[⊥] Institute of Molecular Sciences.

(1) Ginzburg, V. L. *Sov. Phys. JETP* **1957**, *4*, 157.
(2) Fertig, W. A.; Johnston, D. C.; DeLong, L. E.; McCallum, R. W.; Maple, M. B.; Matthias, B. T. *Phys. Rev. Lett.* **1977**, *38*, 987.
(3) Ishikawa, M.; Fischer, Ø. *Solid State Commun.* **1977**, *23*, 37.
(4) Ng, T. K.; Varma, C. M. *Phys. Rev. Lett.* **1997**, *78*, 330.
(5) Bernhard, C.; Tallon, J. L.; Neidermayer, C.; Blasius, T.; Golnik, A.; Brucher, E.; Kremer, R. K.; Noakes, D. R.; Stronach, C. E.; Ansaldo, E. J. *Phys. Rev. B* **1999**, 14099.
(6) Pringle, D. J.; Tallon, J. L.; Walker, B. G.; Trodahl, H. J. *Phys. Rev. B* **1999**, R11679.
(7) Bechgaard, K.; Carriero, K.; Olsen, M.; Rasmussen, F.; Jacobsen, C. S. *Phys. Rev. Lett.* **1981**, *46*, 452.

10.1021/ic001193u CCC: $20.00
Published on Web 02/14/2001

Some years ago we embarked on a systematic examination of transition metal complexes as anions in charge-transfer salts[8] and reported the first molecular superconductor which contained paramagnetic metal ions (and incidentally the first superconductor of any kind containing paramagnetic 3d ions).[9] Subsequently one other molecular system has been reported,[10] and its properties have been measured as a function of temperature, pressure, composition, and applied fields.[11]

The paramagnetic molecular superconductor,[9] initially formulated as β''-(BEDT-TTF)$_4$[$(H_2O)Fe(C_2O_4)_3$]·PhCN (BEDT-TTF = bis(ethylenedithio)tetrathiafulvalene), consists of alternating layers of BEDT-TTF cations and layers containing the complex anions and solvent molecules. It is monoclinic (*C*2/*c*) but, in parallel, an orthorhombic phase (*Pbcn*) developed, in which the H_2O was replaced by K^+ or NH_4^+ while retaining the same overall arrangement of alternating cationic and anionic layers. However, the *Pbcn* derivatives are semiconducting, principally because the packing of the BEDT-TTF is different: in place of the β'' packing motif as found in numerous other superconducting BEDT-TTF charge-transfer salts is an arrangement that we called "pseudo κ",[9] consisting of neutral BEDT-TTF molecules surrounding a (BEDT-TTF$^+$)$_2$ dimer. In both phases the $[Fe(C_2O_4)_3]^{3-}$ anion, together with the H_2O, K^+, or NH_4^+, forms a planar hexagonal honeycomb network, reminiscent of that found in the extensive series of molecular-based bimetallic magnets with stoichiometry $A^I[M^{II}M^{III}(C_2O_4)_3]$, where here A^I is an organic cation such as tetraalkyl- or tetraarylammonium or -phosphonium.[12,13] An important issue arose as to why a similar arrangement of anions should lead to two such different arrangements of the BEDT-TTF cations. Furthermore, a crucial point of detail in relating the crystal and electronic structure of the superconducting phase to its physical properties concerns the mean charge on the BEDT-TTF. This charge is balanced by that of the anion layer, so the determining factor is whether the water molecule is present as H_2O or H_3O^+. The earlier crystallographic work[9] was inconclusive, but the water was assigned as H_2O on considering the O(H_2O)...O(oxalate) distances.

It is clearly of interest to explore other phases with the general formula (BEDT-TTF)$_4$[$AM(C_2O_4)_3$]·solvent, where M is a transition or even nontransition metal ion, to see how the transport and magnetic parameters change with the magnitude of the magnetic moment, and any small systematic changes in intra- and intermolecular distances. It is also important to clarify whether the monoclinic and orthorhombic compounds can be regarded as polymorphs with the same mean charge on the BEDT-TTF cations and, if so, to clarify the physical origin of the polymorphism. Here we report our efforts to prepare materials with other metal ions, the crystal structures of two new compounds with M = Co and Al, and their basic physical characterization by transport and magnetic susceptibility measurements. Additionally, we report Raman spectra of these and the earlier compounds, which show in every case that the (BEDT-TTF)$_4$ unit has a +2 charge, irrespective of the donor packing motif or the salt composition. A comparison of the supramolecular organization of the monoclinic and orthorhombic phases leads to an explanation for the different packing arrangements of the donor cations, based on different spatial distributions of the enantiomeric $[M(C_2O_4)_3]^{3-}$ in the racemic lattices. Preliminary brief accounts of part of this work have appeared.[14,15] It is interesting to note that recently a BEDT-TTF salt with a bimetallic layer anion $[MnCr(C_2O_4)_3]^-$ was reported to be metallic down to 4 K and ferromagnetic below 5.5 K. However, only a partial structure was determined because of disorder in the anion layer, and furthermore the included solvent molecules were not located.[16]

Experimental Section

Synthesis of Starting Materials. Numerous tris(oxalato)metalate(III) salts were synthesized by literature methods for use in the subsequent electrochemical crystal growth of BEDT-TTF charge-transfer salts. For the previously reported salts with M = Fe or Cr, see the published articles for details.[9,14] The following starting materials were also prepared as indicated and recrystallized several times before use. $(NH_4)_3[Ti(C_2O_4)_3]\cdot 10H_2O$,[17] $K_3[Cr(C_2O_4)_3]\cdot 2H_2O$,[18] $(NH_4)_3[Co(C_2O_4)_3]\cdot 3.5H_2O$,[18] $(NH_4)_3[Ru(C_2O_4)_3]\cdot 1.5H_2O$,[19] $K_3[Ru(C_2O_4)_3]\cdot 4.5H_2O$,[20] $(NH_4)_3[Rh(C_2O_4)_3]\cdot 4.5H_2O$,[21,22] $Gd_2(C_2O_4)_3\cdot 10H_2O$,[23] $(NH_4)_3[Al(C_2O_4)_3]\cdot 3H_2O$,[18] $K_3[Al(C_2O_4)_3]\cdot 3H_2O$.[18] The compositions were confirmed by elemental analysis, carried out by University College London Microanalytical Laboratory. BEDT-TTF (Aldrich) was recrystallized from $CHCl_3$, 18-crown-6 (Aldrich) was purified over MeCN, PhCN (Aldrich) was fractionally distilled over P_2O_5 immediately prior to use, and H_2O was also freshly distilled.

Synthesis of BEDT-TTF Charge-Transfer Salts. Crystal growth took place in H-shaped electrocrystallization cells (maximum volume 50 mL) with a Pt electrode in each arm separated by a glass frit in the "H" cross piece. The cathode was protected by a second frit to prevent contamination by reduction products. The cells were washed with aqua regia followed by distilled H_2O and dried thoroughly. The electrodes were cleaned with nitric acid, after which an ac current was passed through them in dilute H_2SO_4, and finally they were washed in distilled H_2O and thoroughly dried.

In each case 100 mg of the tris(oxalato)metalate salt and 200 mg of 18-crown-6 were dissolved in 50 mL of PhCN. For those compounds which finally contain H_3O^+, the anion source was the ammonium salt, and two drops of water were added after rapid stirring. Ten milligrams of solid BEDT-TTF was placed in the anode side of the H-cell, and

(8) Mallah, T.; Hollis, C.; Bott, S.; Kurmoo, M.; Day, P. *J. Chem. Soc., Dalton Trans.* **1990**, 859. Day, P.; Kurmoo, M.; Mallah, T.; Marsden, I. R.; Allan, M. L.; Friend, R. H.; Pratt, F. L.; Hayes, W.; Chasseau, D.; Bravic, G.; Ducasse L. *J. Am. Chem. Soc.* **1992**, *114*, 10722. Marsden, I. R.; Alan, M. L.; Friend, R. H.; Kurmoo, M.; Kanazawa, D.; Day, P.; Bravic, G.; Chasseau, D.; Ducasse, L.; Hayes, W. *Phys. Rev. B* **1994**, *50*, 2118. Kurmoo, M.; Day, P.; Giuonneau, P.; Gaulter, J.; Chasseau, D.; Ducasse, L.; Allan, M. L.; Marsden, I. R.; Bravic, G.; Friend, R. H. *Inorg. Chem.* **1996**, *35*, 4719. Kepert, C. J.; Kurmoo, M.; Day, P. *Inorg. Chem.* **1997**, *36*, 1128. Kepert, C. J.; Kurmoo, M.; Day, P. *J. Chem. Soc., Dalton Trans.* **1997**, 607. Kepert, C. J.; Kurmoo, M.; Day, P. *J. Mater. Chem.* **1997**, *7*, 221.

(9) Kurmoo, M.; Graham, A. W.; Day, P.; Coles, S. J.; Hursthouse, M. B.; Caulfield, J. L.; Singleton, J.; Pratt, F. L.; Hayes, W.; Ducasse, L.; Guionneau, P. *J. Am. Chem. Soc.* **1995**, *117*, 12209.

(10) Kobayashi, H.; Tomita, H.; Naito, T.; Kobayashi, A.; Sakai, F.; Watanabe, T.; Cassoux, P. *J. Am. Chem. Soc.* **1996**, *118*, 368.

(11) Kobayashi, H.; Sato, A.; Arai, E.; Akutsu, H.; Kobayashi, A.; Cassoux, P. *J. Am. Chem. Soc.*, **1997**, *119*, 12392. Sato, A.; Ojima, E.; Akutsu, H.; Kobayashi, H.; Kobayashi, A.; Cassoux, P. *Chem. Lett.* **1998**, 673. Kobayashi, H.; Akutsu, H.; Ojima, E.; Sato, A.; Tanaka, H.; Kobayashi, A.; Casoux, P. *Synth. Met.* **1999**, *103*, 1837.

(12) Decurtins, S.; Schmalla, H. W.; Oswald, H. R.; Linden, A.; Ensling, J.; Gutlich, P.; Hauser, A. *Inorg. Chim. Acta* **1994**, *216*, 65.

(13) Mathioniere, C.; Nuttall, C. J.; Carling, S. G.; Day, P. *Inorg. Chem.* **1996**, *35*, 1201.

(14) Martin, L.; Turner, S. S.; Day, P.; Mabbs, F. E.; McInnes E. *J. Chem. Soc., Chem Commun.* **1997**, 1367.

(15) Martin, L.; Turner, S. S.; Day, P.; Malik, K. M. A.; Coles, S. J.; Hursthouse, M. B. *J. Chem. Soc., Chem. Commun.* **1999**, 513.

(16) Coronado, E.; Galan-Mascaros, J. R.; Gomez-Garcia, C. J.; Laukhin, V. *Nature* **2000**, *408*, 447.

(17) Piper, T. S.; Carlin, R. L. *J. Chem. Phys.* **1961**, *35*, 1800.

(18) Bachar, J. C.; Jones, E. M. *Inorg. Synth.* **1939**, *1*, 35.

(19) Key. D. L.; Larkworthy, L. F.; Salmon, J. E. *J. Chem. Soc. A* **1971**, 371.

(20) Kaziro, R.; Hambley, T. W.; Bunstead, R. A.; Beattie, J. K. *Inorg. Chim. Acta* **1989**, *164*, 85.

(21) Werner, A.; Poupardin, J. *Ber. Dtsch. Chem. Ges.* **1914**, *47*, 1955.

(22) Gillard, R. D.; Laurie, S. H.; Mitchell, R. *J. Chem. Soc. A* **1969**, 3006.

(23) Wendlandt, W. W. *Ann. Chem.* **1958**, *30*, 58.

the remainder of the cell was filled with the filtered PhCN mixture. At a temperature of 295(2) K a constant current of 1 μA was applied across the cell and where crystals grew on the anode they did so over an average of 21 days.

Results of the crystal growth, with the named tris(oxalato)metalate complexes, were as follows. $(NH_4)_3[Ti(C_2O_4)_3]\cdot 10H_2O$: very thin black needles. $K_3[Cr(C_2O_4)_3]\cdot 3H_2O$: no crystals grew over 21 days. $(NH_4)_3[Co(C_2O_4)_3]\cdot 3.5H_2O$: black needle-shaped crystals which were of good enough quality for single-crystal X-ray structural determination and were found to be $(BEDT\text{-}TTF)_4[(NH_4)Co(C_2O_4)_3]\cdot PhCN$, **I**. $(NH_4)_3[Ru(C_2O_4)_3]\cdot 1.5H_2O$: no crystal growth occurred after 28 days. $K_3[Ru(C_2O_4)_3]\cdot 4.5H_2O$: no crystals grew over 21 days. $(NH_4)_3[Rh(C_2O_4)_3]\cdot 4.5H_2O$: a small amount of very small black needles grew over 14 days but formed as aggregates and were unsuitable for physical measurements. $Gd_2(C_2O_4)_3\cdot 10H_2O$: large black plates. $(NH_4)_3[Al(C_2O_4)_3]\cdot 3H_2O$: a small quantity of square plates of very good quality which were suitable for single-crystal X-ray structural determination were found to be $(BEDT\text{-}TTF)_4[(NH_4)Al(C_2O_4)_3]\cdot PhCN$, **II**. $K_3[Al(C_2O_4)_3]\cdot 3H_2O$: no crystals grew over 21 days.

Enantiomericaly Pure Starting Materials. Since tris(oxalato)-metalate complexes are chiral, the opportunity exists in principle to make BEDT-TTF salts containing only a single enantiomer. For example with Λ-$(NH_4)_3[Cr(C_2O_4)_3]\cdot H_2O$ or Δ-$(NH_4)_3[Cr(C_2O_4)_3]$, prepared by literature methods,[24] no crystals grew in the first 12 days, followed by a period of rapid growth for 3 days which yielded a large quantity of black cubes.[14] However, with Λ-$(NH_4)_3[Rh(C_2O_4)_3]\cdot H_2O$ or Λ-$K_3[Cr(C_2O_4)_3]\cdot H_2O$ no crystals had grown after 28 days.

Crystal Structure Determination. For M = Co, compound **I**, a black needle single crystal was mounted on a glass fiber and positioned on a Bruker smart CCD. The quality of the crystal was checked at room temperature from a cell parameter determination which gave an orthorhombic crystal system (a = 10.407(1) Å, b =19.600(1) Å, c = 36.162(1) Å). Then the sample was cooled (4 K min^{-1}) in order to reduce the strong thermal agitation which usually affects the BEDT-TTF/$[M(C_2O_4)_3]^{n-}$ salts at room temperature.[25] The data collection was then run at 150(2) K with graphite-monochromated Mo Kα radiation (λ = 0.71069 Å). The diffraction frames were integrated using the SAINT package[26] and corrected with SADABS.[27] The crystal structures were solved and refined with the SHELXTL-plus programs.[28] For M = Al single plate crystals, X-ray diffraction data were collected at 150-(2) K using an Enraf Nonius Kappa CCD area detector with Mo Kα radiation and an Oxford Cryosystem N_2 open flow cryostat. The structure was solved by direct methods and refined anisotropically on F^2 by full-matrix least squares using SHELX97.[29] All hydrogen atoms were placed in idealized positions and refined using a riding model.

Physical Measurements. Transport Measurements. Transport measurements of low-resistance and metallic samples were made by the four-probe dc method. Two probe measurements were used for samples with high intrinsic resistance where contact effects were assumed to be negligible. Gold wire electrodes were attached to the crystal using Pt paint, and the attached wires were connected to a standard eight-pin integrated circuit plug with Ag paint. Silver paint was not used for contacts to the sample due to the possible formation of AgS at the electrode−crystal interface. The eight-pin plugs were mounted in an Oxford instruments CF200 continuous-flow cryostat and connected to a Hewlett-Packard 3478A digital multimeter.

Magnetic Susceptibility. Magnetic susceptibility data were measured using a Quantum Design MPMS7 SQUID magnetometer. Measurements were made on polycrystalline samples in a gelatine capsule, and the molar susceptibility was corrected for core diamagnetism estimated from Pascal's constants. For the superconducting compounds a strong field exclusion effect was observed when the samples were cooled in zero field to 2 K and a small field of 5 G was applied. Magnetization measurements were then made while heating the sample to 12 K, which was assumed to be above T_c. The Meissner−Ochsenfeld field expulsion effect is observed on keeping the field constant and then measuring the magnetic susceptibility while recooling. Each superconductor showed an increase in magnetization which indicated some flux penetration.

Infrared Spectroscopy. Polarized optical reflectivity of single crystals was recorded at ambient temperature from 800 to 4000cm^{-1} using a Perkin-Elmer 1710 spectrometer fitted with a Spectra Tech microscope and a KRS5 polarizer. Measurements were made with the electric vector both parallel and perpendicular to the edge of the crystal. Ambient and low-temperature reflectivity was measured using a Spectra-Tech IR-plan microscope fitted in the sample chamber of an FT-IR Nicolet Magna 760 spectrometer. Spectra were collected between 600 and 4000 cm^{-1} using an IR light source, MCT detector, KBr beam splitter, and wire grid polarizer with 4 cm^{-1} resolution; between 3500 and 10000 cm^{-1} using a white light source, MCT detector, quartz beam splitter, and NIR/VIS Glan-Thompson polarizer with 32 cm^{-1} resolution; and between 9000 and 12000 cm^{-1} using a white light source, Si detector, quartz beam splitter, and the same polarizer. Single crystals were fixed on a copper sample holder with silicon grease. The crystal face was adjusted to be nearly normal to the incident light using a small goniometer head attached to an Oxford Instruments CF1104S cryostat. The sample was covered by a radiation shield and vacuum shroud with a KBr window. To avoid the sample being contaminated at low temperature, the window of the radiation shield was only opened during measurement. The absolute reflectivity was obtained by comparison with the reflected light from a Au mirror placed close to the sample. At each temperature the reflectivity of this inner mirror was monitored with respect to a gold mirror outside the cryostat chamber. Spectra from 10000 to 32000 cm^{-1} were measured using the same microscope, combined with a multichannel detection system (Atago Macs320) using a xenon lamp light source and Glan-Thompson polarizer.

Raman Spectroscopy. Raman spectra of single crystals were measured at room temperature with a Renishaw Raman Imaging microscope using a He−Ne laser (λ = 632.6 nm) with 10% filter. Samples were measured both parallel and perpendicular to the incident beam and were scanned from 100 to 4000 cm^{-1} while longer scans were performed from 1150 to 1650 cm^{-1} to observe the stretching frequencies of the C=C bonds in BEDT-TTF. Spectra were identical when measured both parallel and perpendicular to the incident beam (in the same plane of the crystal plates or needles) with only minor changes in peak shifts and intensity. Spectra of metallic salts showed considerably more noise and broader absorption than those of the semiconducting samples and of neutral BEDT-TTF.

Results and Discussion

Description of Crystal Structures. A common feature of charge-transfer salts, based on the donor molecule BEDT-TTF, is the spatial segregation of cations and anions into alternating layers, although occasionally "chess board" patterns can appear as with the $[Ge(C_2O_4)_3]^{4-}$ salt.[25] The structures of all of the salts of BEDT-TTF and tris(oxalato)metalate(III) anions with PhCN consist of layers of BEDT-TTF molecules interleaved with anionic layers which contain $[M^{III}(C_2O_4)_3]^{3-}$, PhCN, and cations $A^1 = H_3O^+$, NH_4^+ or K^+. Figure 1 shows an example of the layered structure in one of these salts. Crystal data for the new compounds are presented in Table 1 along with comparative data for other compounds in this series; compounds **I** and **II** are the new salts, and **III**−**VI** are included for structural comparisons. The compound shorthand, **I**−**VI**, is used in the other tables; compound **VII** is that with M = Fe and A = K. As noted in the original work,[9] two distinct phases have been found in this series with monoclinic ($C2/c$) and orthorhombic

(24) Kauffman, G. B.; Sugisaka, N.; Reid, I. K. *Inorg. Chem.* **1989**, *25*, 139.
(25) Martin, L.; Turner, S. S.; Day, P.; Guionneau, P.; Howard, J. A. K.; Uruichi, M.; Yakushi, K. *J. Mater. Chem.* **1999**, *9*, 2731.
(26) *SAINT*, version 4.050; Siemens Analytical X-ray Instruments: Madison, WI, 1995.
(27) Sheldrick, G. M. *SADABS, Empirical Absorption Program*; University of Göttingen: Göttingen, Germany, 1995.
(28) Sheldrick G. M. *SHELXTL-Plus*, release 4.1; Siemens Analytical X-ray Instruments Inc.; Madison, WI, 1991.
(29) Sheldrick, G. M. *SHELXL97*; University of Göttingen: Göttingen, Germany, 1997.

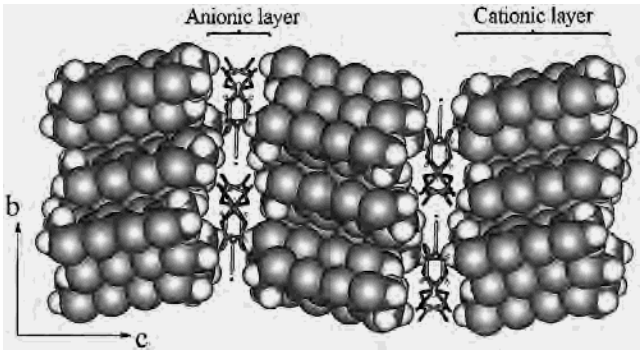

Figure 1. The layered structure in (BEDT-TTF)$_4$[AM(C$_2$O$_4$)$_3$]·PhCN salts.

(*Pbcn*) space groups. Standard ORTEP[30] diagrams with the atom-numbering scheme and 50% thermal ellipsoids for compounds **I** and **II** with M = Co and Al, respectively, both of which have the *Pbcn* structure, are shown in Figures 2 and 3.

Anion Layers. Within each anion layer, the A^I and $[M^{III}(C_2O_4)_3]^{3-}$ groups adopt a "honeycomb" arrangement with a PhCN molecule occupying a hexagonal cavity (Figure 4, top). The PhCN is fully ordered in the monoclinic phases with the C≡N bond directed toward the metal atom of the tris(oxalato) anion, while in the orthorhombic phases it exhibits 2-fold disorder over two static orientations with the C≡N bonds directed toward A^I. The solvent may play a "templating" role in stabilizing the lattice. The area of the cavity is ≈1 Å^2 smaller in the orthorhombic series, because a longer metal to metal distance (c in Figure 4, top right) is needed to accommodate the −C≡N groups on either side, while the cavity in the monoclinic phases is extended along the *b* axis (a in Figure 4, top left). The orthorhombic salt with M = Al and A = NH_4 has a slightly smaller cavity than the corresponding Cr, Fe, and Co salts, having a longer $M^{III}-A^I$ distance (a in Figure 4, top right) yet shorter "b" and "c" distances. The metals are octahedrally coordinated to three bidentate $[C_2O_4]^{2-}$ ligands which confer D_3 point symmetry about the metal. The O atoms of the oxalato ion which are not coordinated to M bound a cavity which is occupied by A^I (Figure 4, bottom). In the monoclinic phase the A^I site is approximately octahedral, whereas in the orthorhombic one it also accommodates two C≡N groups of the PhCN, rendering the site eight coordinate. Furthermore, in the orthorhombic phases the terminal O atoms are not disposed octahedrally because one of the three $[M(C_2O_4)_3]^{3-}$ around the A^I cavity has chirality opposite to that of the other two (Figure 4, bottom right).

The mean A^I-O(oxalate) distances are close to those expected for H-bonded cations for $A^I = NH_4$ or H_3O. In both monoclinic and orthorhombic phases, there are three crystallographically independent $[C_2O_4]^{2-}$ O atoms (O2, O4, and O6 in Figures 2 and 3) at short distances from the cation A. In the monoclinic structures, two of these distances are distinctly shorter than the third (Table 2), which led to the initial suggestion that A^I might be H_2O rather than H_3O^+.

Perhaps the most unusual aspect of these two series of compounds concerns the chirality of the anion layer. Since the $[M^{III}(C_2O_4)_3]^{3-}$ has D_3 point symmetry, it can exist in two enantiomeric forms, Δ and Λ. In the monoclinic phases, each anionic layer consists exclusively of a single enantiomer (Figure 4, left), with the next layer containing only the other enantiomer, to give a ...Δ−Λ−Δ−Λ−Δ−Λ... repeating pattern (where − represents segregation by a layer of donor molecules). By contrast, in the orthorhombic phases each anion layer contains a 1:1 ratio of Δ and Λ enantiomers arranged in alternating rows with a ...ΔΛ−ΔΛ−ΔΛ−ΔΛ... pattern (Figure 4, right). In both phases there is a C2 rotation from one anion layer to the next.

In all compounds the planes of the PhCN solvent molecule are not parallel to the plane defined by the metal atoms in the anionic layer, although to a different extent. In monoclinic materials the solvent is slightly closer to one edge of the hexagonal cavity than in orthorhombic salts. As a result, the phenyl ring of the solvent lies close to the two oxalate ligands which form the base of the hexagonal cavity (see dashed line in Figure 4, top left). The planes of these two ligands make angles of ≈70° to the plane of this cavity, and the phenyl ring is almost parallel to these ligands, thus minimizing the void space around the included solvent molecule. However, in the orthorhombic phases, the phenyl ring is closer to the center of the cavity.

Finally we examine the geometry of the $[M(C_2O_4)_3]^{3-}$ themselves. Figures 2 and 3 shows the atom-numbering scheme used for comparing the bond lengths and angles, a selection of which are listed in Table 3. First, it should be noted that the $M^{III}-O$(oxalate) bonds are significantly shorter in the orthorhombic salts with $A^I = NH_4^+$ than in any of the other structures, while the $M^{III}-O$(oxalate) bond lengths in the Cr salts are slightly longer than those observed in the crystal structure of $(NH_4)_3[Cr(C_2O_4)_3]\cdot 3H_2O$ (1.96 Å at 293 K[28]). The inner O−C distances (not listed) are very similar and close to that expected (1.28 Å at 293 K[31]). The $O-M^{III}-O$ angles in most of the salts are less than the 85° found in the 293 K crystal structure of $(NH_4)_3[Cr(C_2O_4)_3]\cdot 3H_2O$, being slightly smaller in the monoclinic phases (78.5−82.7°) than the orthorhombic ones (80.9−86.2°).

BEDT-TTF Cation Layers. We find two quite different types of packing of the donor molecules. The monoclinic phases adopt a *β″* packing motif, similar to the pressure-induced superconductor (BEDT-TTF)$_3$Cl$_2$·2H$_2$O,[32] while the orthorhombic phases have a novel "pseudo-*κ*" arrangement (Figure 5). In the *β″* phases, the planes of the BEDT-TTF molecules in adjacent layers are twisted with respect to one another, a feature only observed previously in a phase of (BEDT-TTF)$_2$Ag(CN)$_2$.[33] The two crystallographically independent BEDT-TTF are rotated by 61.8° and 63.9°, respectively, measured between the planar central TTF portions of the donors, due to the steric influence imposed upon them by the anion layer. The BEDT-TTF molecules form regular stacks with numerous close S···S distances, those below and close to the van der Waals distance (3.6 Å) being given in Table 4 and marked in Figure 5. The shortest S···S contacts are side-to-side interactions between neighboring stacks (Figure 5a), the shortest being between the S atoms of adjacent outer, six-membered rings. The two crystallographically independent BEDT-TTF molecules each have a twisted and eclipsed conformation. The terminal ethylene C−C bonds and C=C double bond lengths increase slightly

(30) Johnson, C. K. ORTEP. Report ORNL-5138; Oak Ridge National Laboratory: Oak Ridge, TN, 1976.

(31) Van Nierkerk, J. N.; Schoening, F. R. L. *Acta Crystallogr.* **1952**, *5*, 499.

(32) Rosseinsky, M. J.; Kurmoo, M.; Talham, D. R.; Day, P.; Chasseau, D.; Watkin, D.; *J. Chem. Soc., Chem. Commun.* **1988**, 88. Gaultier, J.; Gebrand-Brachetti, S.; Guionneau, P.; Kepert, C. J.; Chasseau, D.; Ducasse, L.; Burrows, Y.; Kurmoo, M.; Day, P. *J. Sol. State Chem.* **1999**, *145*, 496.

(33) Kurmoo, M.; Day, P.; Stringer, A. M.; Howard, J. A. K.; Ducasse, L.; Pratt, F. L.; Singleton, J.; Hayes, W. *J. Mater. Chem.* **1993**, *3*, 1161.

Table 1. Summary of Crystal Data for Selected Compounds with the Stoichiometry $(BEDT\text{-}TTF)_4[A^IM^{III}(C_2O_4)_3]\cdot PhCN$

	I	II	III	IV	V	VI
M^{III}	Co	Al	Fe[a]	Cr[b]	Cr[b]	Fe[a]
A^I	NH_4	NH_4	H_3O	H_3O	H_3O	NH_4
chem formula	$C_{53}H_{41}O_{12}S_{32}CoN_2$	$C_{53}H_{41}O_{12}S_{32}AlN_2$	$C_{53}H_{39}FeN_2O_{13}S_{32}$	$C_{53}H_{37}O_{13}S_{32}CrN$	$C_{53}H_{39}O_{13}S_{32}CrN$	$C_{53}H_{41}FeN_2O_{12}S_{32}$
a/Å	10.340(10)	10.318(7)	10.232(12)	10.240(1)	10.371(2)	10.370(5)
b/Å	19.5016(2)	19.460(4)	20.04(3)	19.965(1)	19.518(3)	19.588(12)
c/Å	35.7684(5)	35.808(8)	34.97(2)	34.905(1)	35.646(2)	35.790(8)
β/deg	90.0	90.0	93.25(11)	93.69(1)	90.0	90.0
V/Å^3	7212.6(14)	7190(5)	7157(13)	7121.6(2)	7216(2)	7270(6)
Z	4	4	4	4	4	4
fw	1982.90	1950.96	1979.78	1973.76	1975.99	1974.61
crys syst	orthorhombic	orthorhombic	monoclinic	monoclinic	orthorhombic	orthorhombic
space group	*Pbcn*	*Pbcn*	*C*2/*c*	*C*2/*c*	*Pbcn*	*Pbcn*
T/K	150(2)	150(2)	120(2)	120(2)	150(2)	120(2)
λ/Å	0.71073 (Mo Kα)	0.71073	0.71073	0.71073	0.71073	0.71073
ρ_{calcd}/g cm^{-3}	1.825	1.798	1.835	1.809	2.137	1.804
μ/mm^{-1}	1.226	1.019	1.207	1.141	1.146	1.187
$R(F_o)$,[c] $[I < 2\sigma(I)]$	$R = 0.0742$	$R = 0.0437$	$R = 0.0416$	$R = 0.0394$	$R = 0.0655$	$R = 0.1557$
$R_w(F_o^2)$[d]	$R_w = 0.2046$	$R_w = 0.1058$	$R_w = 0.0760$	$R_w = 0.0907$	$R_w = 0.1033$	$R_w = 0.3831$

[a] Reference 9. [b] Reference 14. [c] $R = \sum(F_o - F_c)/\sum F_o$. [d] $R_w = \{\sum[w(F_o^2 - F_c2)^2]/\sum[w(F_o^2)^2]\}^{1/2}$.

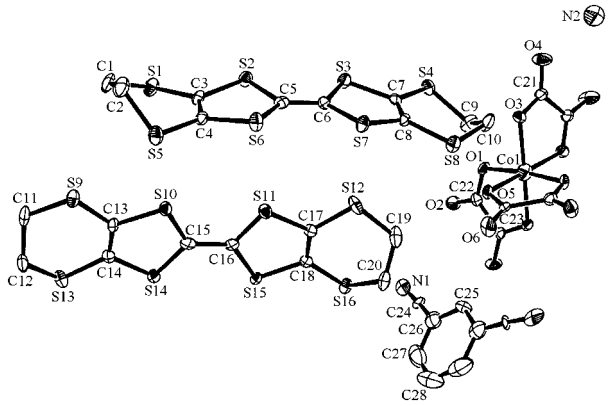

Figure 2. ORTEP[30] diagram with 50% thermal ellipsoids and the atom-numbering scheme for compound **I**, $(BEDT\text{-}TTF)_4[(NH_4)Co(C_2O_4)_3]\cdot PhCN$.

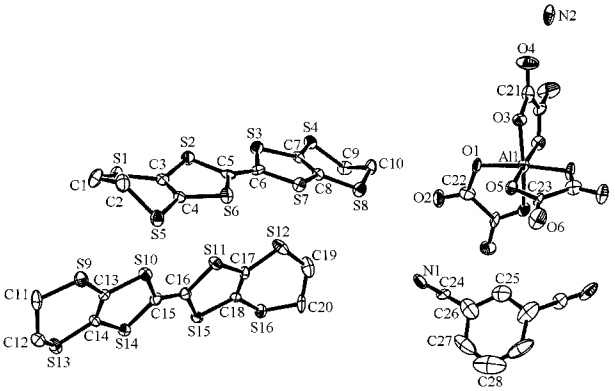

Figure 3. ORTEP[30] diagram with 50% thermal ellipsoids and the atom-numbering scheme for compound **II**, $(BEDT\text{-}TTF)_4[(NH_4)Al(C_2O_4)_3]\cdot PhCN$.

upon cooling from 293 to 120 K, an effect that is usually associated with an increase in charge. In the orthorhombic phases there are again two crystallographically independent BEDT-TTF, each having the twisted and eclipsed conformation at both ends.

Adjacent donor layers are rotated by much greater angles than in the β'' salts at 83.2−85.5° and 85.8−87.8°. The layers consist of face-to-face dimers, each of which is surrounded by six further donors. Neighboring dimers are arranged orthogonal to each other as in the κ-phase salts, though the motif of $(BEDT\text{-}TTF)_2^{2+}$ surrounded by six $BEDT\text{-}TTF^0$ is unique to this series. The closest S···S contact distances occurring between the two molecules of the dimer are 3.43−3.45 Å, and the mode of overlap found in the dimer is not quite the "bond-over-ring" arrangement found in κ-$(BEDT\text{-}TTF)_2X$ phases.[34] The shortest S···S contacts between dimer and monomer are 3.38−3.42 Å, and the shortest distance between monomers is 3.65−3.67 Å. The S···S contacts in the *Pbcn* structures are listed in Table

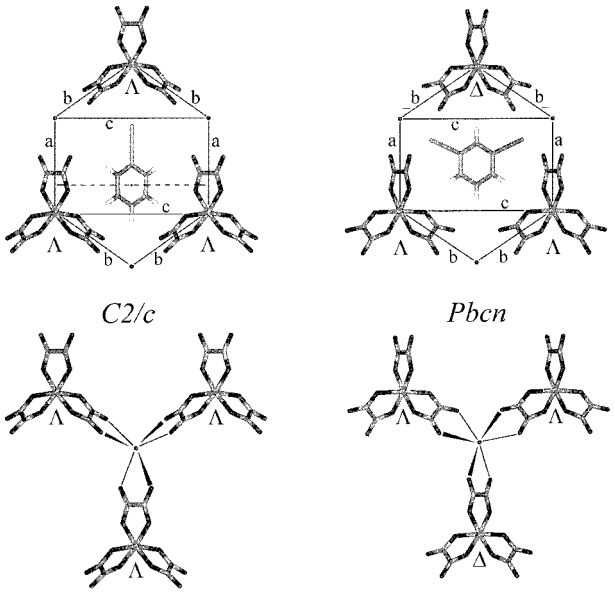

Figure 4. The anionic layer in $(BEDT\text{-}TTF)_4[AM(C_2O_4)_3]\cdot PhCN$ for the monoclinic *C*2/*c* (left) and orthorhombic *Pbcn* (right) structures.

Table 2. Distances (Å) from the Terminal O Atoms of $[M(C_2O_4)_3]^{3-}$ to the Group A in the Title Compounds

compd	*T*/K	04−A	O6−A	O2−A
I	150(2)	2.947(10)	2.981(9)	3.001(9)
II	150(2)	2.977(9)	2.881(9)	2.918(8)
III	120(2)	2.917(5)	2.816(5)	2.952(5)
IV	120(2)	2.960(4)	2.809(4)	3.038(4)
IV	293(3)	3.011(7)	2.845(8)	3.058(7)
V	150(2)	2.891(11)	2.927(11)	2.901(12)
VI	120(2)	2.899(20)	2.919(20)	2.887(20)
VII	120(2)	2.866(8)	2.834(7)	2.885(7)

(34) Yamochi, H.; Kamatsu, T.; Matsukawa, N.; Saito, G.; Mori, T.; Kusonoki, M.; Sakaguchi, K. *J. Am. Chem. Soc.* **1993**, *115*, 11319.

Table 3. Selected Bond Lengths (Å) and Angles (deg) about M in the Title Compounds

compd	*T* /K	M−O3	M−O1	M−O5	O3−M−O3	O5−M−O1
I	150(2)	1.908(5)	1.908(5)	1.913(5)	85.8(3)	86.2(2)
II	150(2)	1.888(6)	1.908(5)	1.906(6)	84.2(4)	83.9(2)
III	120(2)	2.018(3)	2.007(3)	2.011(3)	78.5(2)	80.5(1)
IV	120(2)	1.984(2)	1.985(2)	1.966(2)	81.7(1)	82.7(1)
IV	293(3)	1.983(5)	1.976(4)	1.957(4)	81.2(3)	82.7(2)
V	150(2)	1.973(6)	1.982(6)	1.966(6)	81.5(4)	83.5(3)
VI	120(2)	1.995(10)	2.00(11)	2.012(12)	81.1(6)	80.9(4)
VII	120(2)	2.000(4)	2.021(4)	2.021(4)	80.9(2)	81.0(2)

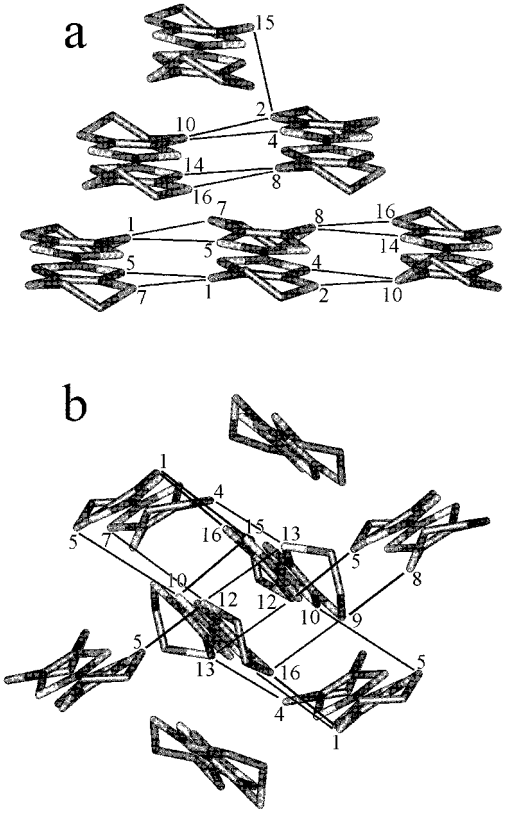

Figure 5. Network of close S···S contacts between BEDT-TTF molecules in (a) monoclinic *C*2/*c* structures with *β*″ packing and (b) orthorhombic *Pbcn* structures.

4b, and a scheme of the contacts is shown in Figure 5. The donor layers are identical, within experimental error, in all the "pseudo-*κ*" structures. A full list of bond lengths, angles, and S···S contact distances for the previously unpublished salts with M = Co and Al are available as Supporting Information in CIF format. The arrangement of the BEDT-TTF molecules is directed by the anion layer and is found to be sensitive to changes in the chirality of $[M(C_2O_4)_3]^{3-}$ and even the solvent molecule.[35]

Anion Cation Interdependency. It has been suggested that weak H-bonding and/or steric interaction between the terminal ethylene groups of BEDT-TTF and the anion layer influences the packing arrangement of the donor layers and, thus, the transport properties of the salts. "Docking" of the donor terminal ethylene groups into cavities between the anions[34] is not a relevant consideration in the present case since there are no cavities of sufficient size when the hexagonal cavity is occupied by a solvent molecule. Consequently, the packing mode of the donor is primarily influenced by short atomic contacts, i.e., H-bonding between the BEDT-TTF terminal ethylene groups and the O atoms of $[M(C_2O_4)_3]^{3-}$. Indeed to preserve this interaction, the $[M(C_2O_4)_3]^{3-}$ units are translated parallel to the *b* axis (see Figure 1) on passing from one layer to the next to an extent that matches the tilt in the long axes of the intervening BEDT-TTF molecules. The fact that H(ethylene)...O(oxalate) contacts are identical at both ends of the donor molecules suggests very strongly that it is these contacts which stabilize the structure.

Table 4. S···S Intermolecular Distances (Å) in the Title Compounds: (a) *C*2/*c* Phases and (b) *Pbcn* Phases[a]

(a) *C*2/*c* Stuctures

	III	**IV**	**IV**
T/K	120(2)	120(2)	293(3)
S1−S5	3.49(1)	3.49(1)	3.56(1)
S1−S7	3.37(1)	3.35(1)	3.40(1)
S2−S10	3.47(1)	3.47(1)	3.57(1)
S2−S15	3.60(1)	3.61(1)	3.65(1)
S4−S10	3.44(1)	3.42(1)	3.51(1)
S8−S14	3.33(1)	3.34(1)	3.37(1)
S8−S16	3.30(1)	3.31(1)	3.35(1)

(b) *Pbcn* Structures

	I	**II**	**V**	**VI**	**VII**
T/K	150(2)	150(2)	150(2)	120(2)	120(2)
S16−S1	3.41(1)	3.38(1)	3.42(1)	3.41(3)	3.40(1)
S12−S13	3.58(1)	3.58(1)	3.58(1)	3.58(3)	3.59(1)
S12−S7	3.49(1)	3.48(1)	3.49(1)	3.49(3)	3.48(1)
S12−S5	3.51(1)	3.50(1)	3.52(1)	3.53(1)	3.52(1)
S15−S1	3.20(1)	3.19(1)	3.20(1)	3.21(3)	3.20(1)
S10−S15	3.45(1)	3.43(1)	3.45(1)	3.45(3)	3.45(1)
S14−S11	3.48(1)	3.46(1)	3.48(1)	3.48(3)	3.48(1)
S10−S5	3.43(1)	3.43(1)	3.41(1)	3.42(3)	3.43(1)
S13−S4	3.43(1)	3.42(1)	3.43(1)	3.46(3)	3.44(1)
S9−S8	3.49(1)	3.49(1)	3.51(1)	3.51(3)	3.51(1)

[a] See Figure 5 for atom numbering.

Because the spatial distribution of the Δ and Λ enantiomers is different in the two sets of compounds, the relative positions of the oxalato O atoms likewise differ. Hence the short atomic contacts with the donor molecules are altered, resulting in the two very different BEDT-TTF packing modes. Given that the distribution of the two $[M(C_2O_4)_3]^{3-}$ enantiomers determines the donor packing motif, it is pertinent to attempt the synthesis of a BEDT-TTF salt starting from a single enantiomer (see synthesis section). Since $[Fe(C_2O_4)_3]^{3-}$ racemizes rapidly, crystals were grown with Cr and Co complexes. When racemic $[M(C_2O_4)_3]^{3-}$ was used crystal growth started quickly whereas for the chirally pure materials no crystals grew over the first 12 days in the case of Cr. Presumably as the anion racemized in solution, crystals of the orthorhombic phase grew over the next few days. However, in contrast to the orthorhombic phases grown from racemic $(NH_4)_3[M(C_2O_4)_3]\cdot xH_2O$ which all contain NH_4^+ (Table 1), the orthorhombic crystals resulting from this in situ racemization process contain H_3O^+. Clearly the nucleation and crystal growth of these phases is a very subtle process in which the packing mode of the two chiral enantiomers of $[M(C_2O_4)_3]^{3-}$ is a crucial factor.

(35) Turner, S. S.; Day, P.; Malik, K. M. A. Hursthouse, M. B. *Inorg. Chem.* **1999**, *38*, 3543.

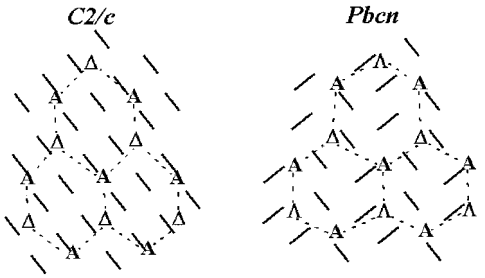

Figure 6. Schematic relationship between the BEDT-TTF donors viewed along their long axes (thick lines) and the anionic "honeycomb" layer (dashed lines) for monoclinic *C*2/*c* (left) and orthorhombic *Pbcn* (right) structures.

Figure 6 shows a schematic representation of the position of the BEDT-TTF molecules with respect to the anion hexagonal layer. In those structures determined at 120 K, the three shortest O(oxalate)...H(donor) distances are from terminal $[C_2O_4]^{2-}$ oxygen atoms. The $-CH_2CH_2-$ terminal group interacts with four sites in the anion layer of the monoclinic structure: over the O adjacent to the phenyl ring of the PhCN, over the C≡N group of PhCN, and above the M^{III} and in the space between PhCN and one of the $[C_2O_4]^{2-}$ units. In the orthorhombic salts the $-CH_2CH_2-$ groups also lie close to four sites in the anion layer: the two BEDT-TTF^0 ethylene groups are below the PhCN, while those of the BEDT-TTF dimer lie close to the O of the $[M^{III}(C_2O_4)_3]^{3-}$. The close O···H contacts are similar in all the orthorhombic structures, the shortest being between 2.3 and 2.7 Å. In Figure 6 (left) it is evident that the donor molecules which are H-bonded to an anionic layer of single $[M(C_2O_4)_3]^{3-}$ enantiomers gives rise a well-ordered packing motif of identically orientated donors. In this case interaction with a pure Δ anionic layer gives a donor layer consisting of stacks propagating from bottom left to top right of Figure 6; interaction with a layer of the Λ enantiomer would give rise to an identical donor packing ranging from bottom right to top left. From Figure 6 (right), it can be seen that in the orthorhombic case those donor dimers which are close to Δ enantiomers of the oxalato anions have similar orientations to those in Figure 6 (left). Similarly those dimers in Figure 6 (right) which are close to Λ oxalato enantiomers have the same orientations to those in the monoclinic structure which interact with a purely Λ anionic layer.

The formal charge associated with each BEDT-TTF donor molecule is an important aid to understanding the physical properties of these salts. The presence of more than one crystallographically independent BEDT-TTF molecule is found in many charge-transfer salts, carrying with it the possibility of charge localization. We have used both bond length analysis and Raman spectroscopy to estimate the charges associated with the donor molecules.

Bond Length Analysis. Molecular orbital calculations on the BEDT-TTF molecule in various oxidation states indicate that it is the central region of the BEDT-TTF molecule which donates charge upon oxidation, and also undergoes the largest changes in bond lengths, which vary monotonically and approximately linearly with charge. The charges on the BEDT-TTF cations have been estimated from the length of the central C=C bond[36] and, more recently, through a systematic search of the Cambridge Crystallographic Database to compare the formal charge from stoichiometry with the bond lengths in the central TTF portion of the molecule.[37] Increased oxidation lengthens the C=C bonds which are bonding with respect to the HOMO. There are also smaller changes to the bond lengths in the outer six-membered rings of the molecule, but structural disorder and increased thermal vibration impede the observation of any systematic variation.

Table 5. The Charge, *Q*, Calculated from C=C and C−S Bond Distance for the Two Crystallographically Independent BEDT-TTF Molecules (a and b); the Semiconducting Activation Energies of the *Pbcn* Phases

compd	*T*/K	*Q*(BEDT-TTF_a)	*Q*(BEDT-TTF_b)	E_{act}/eV
I	150(2)	+0.2	+1.0	0.225
II	150(2)	+0.1	+0.8	0.222
III	120(2)	+0.4	+0.5	n/a
IV	120(2)	+0.6	+0.7	n/a
IV	293(3)	+0.3	+0.4	n/a
V	150(2)	+0.0	+0.8	0.153
VI	120(2)	−0.1	+0.8	0.140
VII	120(2)	+0.1	+0.8	0.141

Guionneau, Kepert, et al.[37] showed that the charge *Q* on a BEDT-TTF molecule can be estimated using an empirical relationship between *Q* and the BEDT-TTF C−S and C=C bond lengths. This relationship provides an estimate of the charge residing on a BEDT-TTF molecule with approximately twice the precision of the earlier correlations.[36] However, it should be noted that the assumption of a linear relationship relies upon single structures for salts containing BEDT-TTF^0 and BEDT-TTF^{2+}. Taking into account the standard deviations in bond lengths we estimate that this method is capable of obtaining charges to an error of 10%. From Table 5 it is clear that in all the salts with formulas β''-(BEDT-TTF)$_4$[$AM(C_2O_4)_3$]·PhCN the two crystallographically independent BEDT-TTF molecules have charges close to +0.5 (average +0.48). Thus A is always monopositive, indicating that the H_xO unit is in fact H_3O^+. This conclusion is also consistent with the site symmetry of the H_xO site (D_3) with three H-bonds to the terminal O atoms of the neighboring $[M(C_2O_4)_3]^{3-}$. It also suggests the more commonly observed 3/4 filling of the four BEDT-TTF HOMO bands rather than 5/8 filling, which would be required if BEDT-TTF had +0.75 formal charge. The presence of H_3O^+ in the "pseudo-κ" salts is likewise supported since the two BEDT-TTF molecules have charges of approximately 0 and +1 (±0.1). The BEDT-TTF^+ form the face-to-face dimers which are surrounded by six neutral BEDT-TTF. Spin-pairing between the radical cations forming the dimers is confirmed by the magnetic susceptibility measurements, which contain no contribution from BEDT-TTF.

Raman Spectroscopy. Raman spectroscopy provides an additional means for determining the charges on BEDT-TTF molecules by monitoring the two symmetric Raman active C=C stretching frequencies between 1400 and 1550 cm^{-1} (designated υ_3 and υ_4[38]). Table 6 lists υ_3 and υ_4 for each of the salts and the calculated charge on each BEDT-TTF molecule according to the relations given by Wang et al.[38] Figure 7 shows examples of Raman spectra for the *Pbcn* (Figure 7a) and *C*2/*c* (Figure 7b) phases. Raman spectra of the β''-phase salts all contain very strong υ_4 peaks between 1466 and 1475 cm^{-1}, and a slightly weaker υ_3 peak between 1492 and 1498 cm^{-1}. The charge $Q(\upsilon_3)$ calculated from υ_3 is close to 0.5^+ in all cases (Table 6), while those calculated from the υ_4 peaks are slightly lower (0.38^+ to 0.48^+). The *Pbcn* series all show intense υ_4 peaks in the region 1493−1496 cm^{-1} characteristic of BEDT-

(36) For example, see: Abboud, K. A.; Clevenger, M. B.; de Oliveira, G. F.; Talham, D. R. *J. Am. Chem. Soc.* **1993**, 1560.

(37) Guionneau, P.; Kepert, C. J.; Chasseau, D.; Truter, M. R.; Day, P. *Synth. Met.* **1997**, *86*, 1973.

(38) Wang, H. H.; Ferraro, J. R.; Williams, J. M.; Geiser, U.; Schleuter, J. A. *J. Chem. Soc., Chem. Commun.* **1994**, 1893.

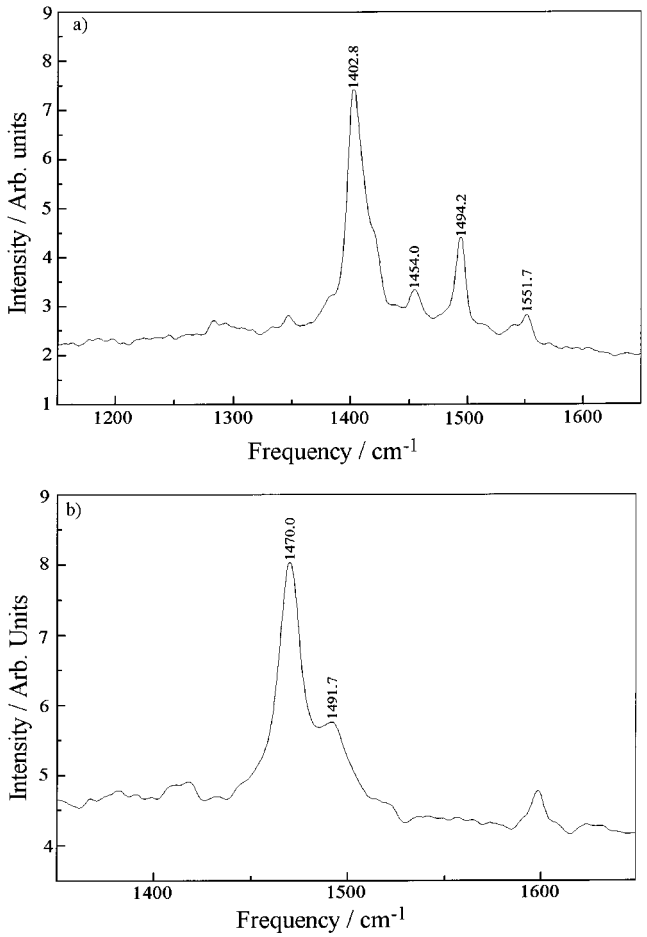

Figure 7. Raman spectra of (a) compound **I** with an orthorhombic *Pbcn* structure and (b) compound **IV** with a monoclinic *C*2/*c* structure.

Table 6. Raman Active Vibrational Frequencies (υ_3 and υ_4) for the C═C Bonds in BEDT-TTF and Calculated Charges

compd	ν_3	ν_4	$Q\nu_3$	$Q\nu_4$
I	1551.7	1494.2	−0.15	0.15
	1454.0	1402.8	0.99	1.19
II	1550.8	1493.2	−0.14	0.17
	1453.0	1403.7	1.00	1.18
		(1510.6)		
III	1495 (sh)	1475.0	0.51	0.37
IV	1491.7	1470.0	0.55	0.43
V	1552.6	1494.2	−0.16	0.15
	1454.0	1402.8	0.99	1.19
VI	1552.1	1494.6	−0.15	0.15
	1454.2	1420.0	0.99	1.00
		(1510.8)		
BEDT-TTF^0	1552.6	1495.1	−0.16	0.15
		(1511.5)		

TTF^0 and at 1403−1423 cm^{-1} indicating BEDT-TTF$^+$. In addition slightly weaker υ_3 peaks occur between 1549 and 1553 cm^{-1} (BEDT-TTF^0) and from 1454 to 1470 cm^{-1} (BEDT-TTF$^+$). The relations of Wang et al.[38] give charges very close to zero (±0.025) for those molecules thought to be BEDT-TTF^0, while for peaks assigned to BEDT-TTF$^+$, the value of $Q(\upsilon_4)$ is slightly larger than that of $Q(\upsilon_3)$, but in all cases gives charges close to +1. In conclusion the Raman spectra confirm the charges estimated from the bond lengths, indicating that all salts contain a (BEDT-TTF)$_4^{2+}$ moiety with molecule A being monovalent.

Infrared Reflection Spectroscopy. In the infrared reflection spectra of all the monoclinic and orthorhombic phases, peaks are observed in the regions 1264−1286 and 1307−1354 cm^{-1} (O−C−O stretching vibration), 1364−1417 cm^{-1} (O−C−O symmetric stretch), and 1636−1664 cm^{-1} (O−C−O asymmetric stretch). Characteristic features of the spectra of the β''-phases are peaks at 872−884 cm^{-1} while pseudo-κ phases have peaks at ca.772, 924−971, 1010−1026, 1036−1076, 1082−1124, 1147−1776, and 1204−1240 cm^{-1}. Very sharp bands are observed in all pseudo-κ salts between 802 and 840, 1307 and 1354, 1364 and 1417, and 1636 and 1664 cm^{-1}.

In addition to sharp peaks due to localized molecular vibrations, the infrared reflectivities of the metallic β''-phases contain broad reflectivity edges at the plasma frequency. The reflectivity is only weakly dependent on whether the polarization is parallel and perpendicular to the axis of the needlelike crystals, both being measured in the same plane as the 2D BEDT-TTF conducting network. As expected, the reflected intensity increases slightly with decreasing temperature. The onset of high reflectivity defines the plasma frequency as 5000 ± 200 cm^{-1}. Finally, for the materials prepared with M = Ti or Gd, the infrared spectra did not show any peaks which could be assigned to the oxalate ligands and so no further physical properties were investigated.

Table 7. Curie (C) and Weiss (θ) Magnetic Constants for the Title Compounds

	C (emu K mol^{-1})		
compd	obsd	calcd spin-only	θ/K
I	n/a	0.00	n/a
II	2.84	3.001	+0.86
III	4.38	4.377	−1.29
IV		1.876	
2−150 K	1.96		−0.21
150−270 K	2.91		−61.5
V	1.73	1.876	+0.88
VI	4.37	4.377	+0.11
VII	4.44	4.377	−0.25

Conductivity Measurements. The monoclinic phases show metal to superconducting transitions,[9,14] but all the orthorhombic phases, including the new compounds, are semiconducting with resistivity increasing exponentially with decreasing temperature. The activation energies for the semiconductors are listed in Table 5. As shown above, the BEDT-TTF molecules in the orthorhombic series form dimers of BEDT-TTF$^+$ surrounded by BEDT-TTF^0. The neutral molecules have filled HOMOs, while the monopositive donors have half-filled HOMOs. The dimerization of the BEDT-TTF$^+$ molecules leads to the formation of a full band and an empty band separated by an energy gap.

Magnetic Properties. All the compounds that contain paramagnetic 3d ions have moments close to that expected for spin only contributions. In addition, the superconducting salts show both flux exclusion and the Meissner−Oschenfeld flux expulsion effect when cooled in fields below 50 G. Table 7 lists the Curie and Weiss constants extracted from plots of inverse molar susceptibility versus temperature. All the Weiss constants are close to zero, indicating that there is very little interaction between paramagnetic centers. The plot of β''-(BEDT-TTF)$_4$[(H$_3$O)Cr(C$_2$O$_4$)$_3$]·PhCN shows a distinct change in slope at ∼150 K, accompanied by a sharp drop in infrared reflectivity when the electric vector is perpendicular to the needle axis. Above 150 K the Curie constant is higher than anticipated for Cr^{3+} ($S = {}^3/_2$), and the Weiss constant of −61.5 K suggests antiferromagnetic interaction between metal centers. However, the crystal structure of the (H$_3$O)Cr salt has been solved at both 120 and 293 K with no evidence for a structural phase transition.

Conclusions

We have compared the structural and physical characteristics of a number of charge-transfer salts with the general formula $(BEDT\text{-}TTF)_4[A^IM^{III}(C_2O_4)_3]\cdot PhCN$ where $A^I = NH_4^+$, K^+, or H_3O^+ and M^{III} = Cr, Fe, Co, or Al, the compounds with M = Co and Al being new members of this series. Analysis of the C=C and C−S bond lengths and Raman spectra of the BEDT-TTF molecules shows that, in all the examples containing water, it is in the form of H_3O^+ and not H_2O. The compounds fall into two categories. Monoclinic phases with $A^I = H_3O$ and M^{III} = Cr and Fe have β'' packing of the BEDT-TTF and are room temperature metals, becoming superconducting at 5.5 K (Cr) and 8.3 K (Fe). Since the magnetic moment of the 3d ion in the Fe ($S = {}^5/_2$) compound is larger than in the Cr ($S = {}^3/_2$), it is clear that the presence of a higher paramagnetic moment in the lattice does not inhibit the superconductivity. A second series of phases found for $A^I = NH_4$, K, H_3O and M^{III} = Cr, Fe, Co, Al are orthorhombic. The BEDT-TTF bond lengths and Raman spectra confirm the presence of two types of donor molecule: face to face dimers with a charge of +1 per molecule surrounded by molecules with charges close to zero. All the members of the orthorhombic series are semiconducting with low activation energies between 0.14 and 0.22 eV.

Both the monoclinic and orthorhombic phases consist of alternating layers of BEDT-TTF and the tris(oxalato)metalate-(III) anions. The anion layers always consist of approximately hexagonal arrays of A and M, bridged by the $[C_2O_4]^{2-}$ with PhCN occupying the hexagonal cavities. Both structures are achiral and contain equal proportions of the enantiomers of $[M(C_2O_4)_3]^{3-}$. However, in the monoclinic phase each layer contains one enantiomer with nearest neighbor layers having opposite chirality whereas each layer of the orthorhombic phase contains enantiomers arranged in alternate rows. As a consequence, while the cavity occupied by A^I consists of an approximately octahedral array of O atoms, that of the orthorhombic phase has a more irregular shape, leaving space for the N atom of the PhCN to coordinate to A^I, bringing the coordination number to 7. Furthermore the array of O atoms which forms the interface with the BEDT-TTF layers differs greatly and, via H-bonding, promotes the different donor packing modes. In one case (A = H_3O; M = Cr) both orthorhombic and monoclinic phases have been found. Our belief is that this constitutes the first example in any compound where polymorphism arises from different spatial distributions of chiral enantiomers in a racemic crystal.

Clearly it will be of great interest to prepare BEDT-TTF salts analogous to the bimetallic tris(oxalato)metalate (II, III) molecular based magnets[12,13] because there would be a good chance of combining metallic behavior or superconductivity with long-range magnetic order in a molecular lattice. Efforts are continuing along these themes.

Acknowledgment. This work has been supported by the UK Engineering and Physical Sciences Research Council and the European Commission Training and Mobility of Researchers Program. We are also grateful to the British Council and Monbusho exchange program (grant to L.M.) and to Dr. W. Hayes (Clarendon Laboratory, Oxford) for access to the infrared spectrometer.

Supporting Information Available: Tables of atomic positional parameters, anisotropic thermal parameters, interatomic contacts, and complete bond distances and angles for compounds **I** and **II** in CIF format. This material is available free of charge via the Internet at http://pubs.acs.org.

IC001193U